

ARTICLE

Electron Affinities of the Early Lanthanide Monoxide Molecules[†]Chao-xian Chi^a, Hua Xie^b, Ran Cong^b, Zi-chao Tang^{b*}, Ming-fei Zhou^{a*}*a. Department of Chemistry, Shanghai Key Laboratory of Molecular Catalysts and Innovative Materials, Fudan University, Shanghai 200433, China**b. State Key Laboratory of Molecular Reaction Dynamics, Dalian Institute of Chemical Physics, Chinese Academy of Sciences, Dalian 116023, China*

(Dated: Received on September 27, 2011; Accepted on October 9, 2011)

The photoelectron imagings of LaO^- , CeO^- , PrO^- , and NdO^- at 1064 nm are reported. The well resolved photoelectron spectra allow the electron affinities to be determined as 0.99(1) eV for LaO , 1.00(1) eV for CeO , 1.00(1) eV for PrO , and 1.01(1) eV for NdO , respectively. Density functional calculations and natural atomic orbital analyses show that the 4f electrons tend to be localized and suffer little from the charge states of the molecules. The photodetached electron mainly originates from the 6s orbital of the metals. The ligand field theory with the $\delta=2$ assumption is still an effective method to analyze the ground states of the neutral and anionic lanthanide monoxides.

Key words: LaO , CeO , PrO , NdO , Electron affinity, Photoelectron imaging, Density functional calculation, Ligand field theory

I. INTRODUCTION

During the past years, considerable attention has been paid to lanthanide-containing systems for their practical and potential usage in chemistry, biology, medicine, and high technological industry [1–3]. Characterizing the physical and chemical properties of lanthanide compounds possess special challenge to both applied and theoretical research. The partially filled 4f, 5d, and 6s orbitals and the strong spin-orbit interactions lead to a large number of energetically adjacent electronic states which strongly perturb each other. Different molecular states of the same 4f configuration often have similar rotational constants and vibrational frequencies, which are no longer effective to establish electronic energy diagram from the spectroscopic data. As in the theoretical research, the large contributions from the relativity and electron correlation have to be accounted in the electronic structure calculation of lanthanide compounds [4]. Many of the 4f open shell systems with a large number of low lying electronic states require multireference wavefunctions and spin-orbit effects included for a proper description.

The lanthanide monoxides are one kind of the simplest lanthanide-containing species. The understanding of their electronic structures is of particular importance to gain deep insight into the properties of molecular

systems containing f elements. The lanthanide monoxide molecules have been extensively investigated experimentally using spectroscopic methods including laser based emission and absorption and theoretically with ligand field theory (LFT) as well as various *ab initio* (MCSCF-MRCI, CISD etc.) and density functional theory methods [5–37]. The electron affinities (EAs) of LaO (0.97 ± 0.10 eV) and GdO (1.19 ± 0.10 eV) were reported from photoelectron spectroscopic studies [38, 39]. Density functional calculations using the hybrid B3LYP functional underestimated the electron affinities of LaO and GdO . In the present work, the early lanthanide metal monoxides including La, Ce, Pr and Nd are investigated using the electron velocity map imaging at 1064 nm (1.165 eV). Accurate EAs of these four lanthanide monoxide molecules are reported.

II. EXPERIMENTAL AND COMPUTATIONAL METHOD

The experiments were carried out using a collinear velocity map photoelectron imaging analyzer with a laser vaporization source. The apparatus has been described in detail elsewhere [40]. Briefly, the earlier lanthanide monoxide anions were generated by pulsed laser vaporization of pure metal targets. The helium carrier gas (99.9%) at stagnation pressures between 300 and 500 kPa expands into vacuum through a pulsed (10 Hz) general valve. The oxygen comes from contamination on the target surface or in the carrier gas. After an adiabatic expansion, the anions are analyzed using a time-of-flight mass spectrometer. In the imaging experiments, the anions were introduced into the laser

[†]Part of the special issue for “the Chinese Chemical Society’s 12th National Chemical Dynamics Symposium”.

*Authors to whom correspondence should be addressed. E-mail: mifzhou@fudan.edu.cn

detachment region and interacted with the laser beam from a Nd:YAG laser (1064 or 532 nm). The laser propagated perpendicularly to the anion beam axis with a polarization vector parallel to the imaging plane. The photoelectrons in the detachment region were extracted by a modified collinear VMI electrode based on the original design of Eppink and Parker and then were mapped onto a imaging detector consisting of a 40 mm diameter microchannel plate assembly and a phosphor screen [41]. The two-dimensional (2D) images on the phosphor screen were recorded by a CCD camera. All the photoelectron images were reconstructed using the BA-SEX program [42], which yielded both the photoelectron kinetic energy spectra and anisotropy parameters. The energy resolution is better than 40 meV at electron kinetic energy (eKE) of 1 eV. Due to the cooling process inherent in the adiabatic expansion, the vibrational temperatures of the anions in the ion beam are low and most of the anions are in their vibrational and electronic ground state prior to the detachment process.

Theoretical calculations were performed to elucidate electronic structures of the anionic and neutral lanthanide monoxides by using the Gaussian 09 program [43]. The calculations were performed at the level of density functional theory (DFT) with the B3LYP method [44, 45]. Several other density functions were also employed for comparison, including BP86 and the new M06 and M06-2X hybrid functionals implemented in the Gaussian 09 program [46–48]. Stuttgart/Dresden ECP, *i.e.*, SDD basis set [34, 35, 49], which is a triple-zeta basis set with 28-core-electrons and takes into account of the scalar relativistic effects, is used for the metal atoms. The aug-cc-pVTZ basis set is used for O [50, 51]. The integral grid used for DFT calculations is a pruned 99.59×10^3 grid. Different spin states were evaluated. Harmonic vibrational frequencies were calculated at the same level of theory to verify the nature of the stationary points and to get the zero-point energy. The electron affinity (EA) in each case was calculated as energy difference between the optimized anionic structure and the optimized neutral one. A natural bond orbital (NBO) analysis of the anionic and neutral clusters was carried out to give a rigorous description of the molecular wavefunction close to the chemical concept of the Lewis structures [52, 53].

III. RESULTS AND DISCUSSION

Figure 1 shows the photoelectron images of LaO^- , CeO^- , PrO^- , and NdO^- at 1064 nm (1.165 eV), respectively. The raw image (top on the left) shows the 2D projection of the 3D laboratory frame photoelectron probability density onto the plane of the imaging detector, and the reconstructed image (bottom on the left) obtained by reconstructing from the raw image using the Abel inversion [54], displays the 2D cuts through the respective 3D velocity distribution. The double ar-

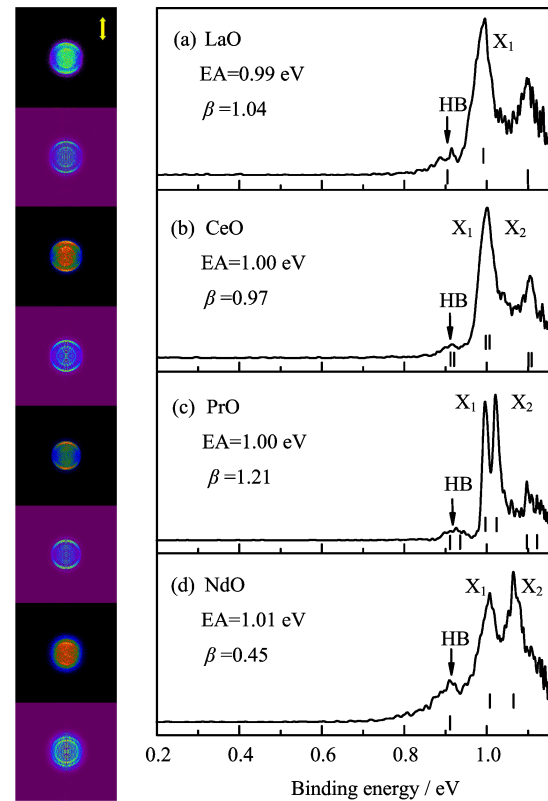


FIG. 1 Photoelectron images and spectra for LaO^- , CeO^- , PrO^- , and NdO^- obtained at 1064 nm (1.165 eV). The left side shows the raw photoelectron image (top on the left) and the reconstructed one (bottom on the left) after inverse Abel transformation. The double arrow shows the direction of the laser polarization. The experimental conditions of the four species are similar and allow a direct visual comparison of the spectral features.

row in the raw image indicates the direction of the laser polarization. Photoelectron spectra and the PADs are obtained by integrating the reconstructed images, including the necessary Jacobian factors. The photoelectron spectra are plotted versus electron binding energy, $e\text{BE} = h\nu - e\text{KE}$ and allow for direct comparison of imaging data.

The images in Fig. 1 are acquired under similar experimental conditions and allow a direct visual comparison of the spectral features. Every ring in the reconstructed image corresponds to one photodetachment transition and their radii reflect the velocities of the outgoing photoelectrons. The large radius represents high kinetic energy of electrons and low binding energy to the anion, according to the function mentioned above. There is no obvious change of the radius of the outer main rings from LaO^- to NdO^- , reflecting that the four lanthanide monoxides have similar electron affinities and the increased f electrons and relativistic effects have little effect on the EAs of the four species. The higher bars in the photoelectron spectra correspond to the electronic states. The X_1 and X_2 designate the ground and the

TABLE I Experimental electron binding energies (eBEs) (in eV), the anisotropy parameters β for the main transitions, and term energies T_e (in cm^{-1}).

		eBE _{expt.}	β	T_e^{a}	T_e^{b}	Final state	Final configuration ^c	$(J_f, \Omega_f)_{J_a}^{\text{c}}$	$(J_f, J_a)^{\text{d}}$
LaO ⁻	X ₁	0.99(1)	1.04(3)	0	0	${}^2\Sigma^+$	$\sigma^2\sigma^*{}^1\text{f}^0$		
CeO ⁻	X ₁	1.00(1)	0.97(5)	0	0	$\Omega=2$	$\sigma^2\sigma^*{}^1\text{f}^1$	${}^2\text{F}_{2.5}(2.5, 2.5)_2$	(2.5, 2)
	X ₂				84.5 [57]	$\Omega=3$		${}^2\text{F}_{2.5}(2.5, 2.5)_3$	(2.5, 3)
PrO ⁻	X ₁	1.00(1)	1.21(3)	0	0	$\Omega=3.5$	$\sigma^2\sigma^*{}^1\text{f}^2$	${}^3\text{H}_4(4, 4)_{3.5}$	(4, 3.5)
	X ₂	1.02(1)	1.04(3)	202	220 [60]	$\Omega=4.5$		${}^3\text{H}_4(4, 4)_{4.5}$	(4, 4.5)
NdO ⁻	X ₁	1.01(1)	0.45(1)	0	0	$\Omega=4$	$\sigma^2\sigma^*{}^1\text{f}^3$	${}^4\text{I}_{4.5}(4.5, 4.5)_4$	(4.5, 4)
	X ₂	1.06(1)	0.30(3)	462	473.7 [62]	$\Omega=5$		${}^4\text{I}_{4.5}(4.5, 4.5)_5$	(4.5, 5)

^a This work.

^b Previous experimental work.

^c Ref.[22]. J_f is the angular momentum of the f^n core and J_a is the total atomic angular momentum.

^d Dominant state wave function expressed in $|J_f, J_a\rangle$ Hund's case (c) basis set, see Ref.[23].

TABLE II Summary of the experimental EA (in eV) and vibrational frequencies (in cm^{-1}) of LnO (Ln=La, Ce, Pr, Nd), together with the previous experimental studies for vibrational frequencies of the neutrals. The theoretical results are also listed for comparison.

	Experiment			B3LYP		BP86		M06		M06-2X	
	EA	ω	ω^{a}	EA	ω	EA	ω	EA	ω	EA	ω
LaO	0.99(1)	851(30)	813 [37]	0.88	828.5	0.94	818.4	1.05	858.1	0.97	857.2
CeO	1.00(1)	836(30)	808.3 [58, 59] 862 [37]	0.88	840.3	0.91	828.1	1.06	869.5	0.99	867.3
PrO	1.00(1)	815(30)	816.9 [58, 59]	0.88	845.3	0.89	794.7	1.01	872.2	1.02	875.8
NdO	1.01(1)		814.2 [58, 59] 834.08 [62]	0.91	840.0	0.86	757.0	0.93	773.7	1.02	873.1

^a Previous experimental studies.

first excited states, respectively. The lower bars near the energy window correspond to vibratioanl levels of the respective electronic states. The lower bars on the lower binding energy side of the main transitions are the hot bands (HB). The results are summarized in Table I.

A. LaO⁻

The peak X₁ in the photoelectron spectrum of LaO⁻ is assigned to the $\text{X}^1\Sigma^+(v''=0)\rightarrow\text{X}^2\Sigma^+(v'=0)$ transition [31, 39, 55], i.e., the transition from the ground vibronic state of the LaO⁻ to the ground vibronic state of LaO. The ligand field theory predicated that the ground state of neutral LaO molecule has an electronic configuration of $\sigma^2\sigma^*{}^1\text{f}^0$ (Table I) [22], in which the $\sigma^*{}^1\text{f}^0$ part is derived from the free La²⁺ 6s4f⁰ configuration. As for the anion, the extra electron adds to the singly occupied σ^* or 6s orbital to form the $\sigma^2\sigma^*{}^1\text{f}^0$ configuration. The electron affinity of LaO is determined to be 0.99(1) eV which is very close to the value (0.97(10) eV) got previously from the photoelectron spectrum of LaO⁻ [39]. The peak centered around 1.10 eV with an anisotropy parameter β value of 0.24(4), is about 0.11 eV (851(30) cm^{-1}) higher in

electron binding energy than that of peak X₁, which is similar to the vibrational frequency of ground state LaO (813 cm^{-1}) (Table II) [37]. We assign this peak as the transition to the first vibrational excited state of LaO $\text{X}^2\Sigma^+(v'=1)$. The peak centered around 0.90(2) eV with $\beta=1.38(5)$, having a band gap of about 0.09 eV with the peak X₁, is also presented in the photoelectron spectrum reported previously and is assigned as the hot band [39], corresponding to the transition from the first vibrational excited state of LaO⁻ to the ground vibronic state of LaO.

B. CeO⁻

The photoelectron spectrum of CeO⁻ shown in Fig.1(b) also exhibited three peaks. The band centered around 1.00 eV is assigned as the transition from ground vibronic state of the CeO⁻ (X₁2.5 ($J_a=2.5, \Omega=2.5$)) to the ground state of the CeO (X₁2($J_a=2, \Omega=2$)) [52, 56]. It should be noted that the CeO, PrO, and NdO are in the Hund's case (c) coupling limit and are characterized by the projection of the electronic angular momentum along the internuclear axis Ω and the total angular momentum J [56]. The ligand field theory (LFT)

approaches have established the approximate relationship among Ω , J and the atomic angular momentum for Ln^{2+} . As for the CeO case, the Russell-Saunders term for the ground state of the $4f^1$ electron core is $^2\text{F}_{2.5}$, which combines with 6s electron to give total atomic angular momentum $J_a=2$ and 3. The Ω values are then obtained by the projection of J_a on the internuclear axis. The two lowest lying states are characterized as X_{12} ($J_a=2$, $\Omega=2$) ($E=0 \text{ cm}^{-1}$) and X_{23} ($J_a=3$, $\Omega=3$) ($E=84.452 \text{ cm}^{-1}$) [57]. The separation of the ground state and the first excited state is very small and the two states differ only in the orientation of the angular momenta of the 4f electron core and the 6s electron, indicating that the coexistence of the transition to the first excited state X_{23} ($J_a=3$, $\Omega=3$) of CeO can not be ruled in our spectrum. The two transitions may merge into one band due to the limited spectra resolution and the abundance of rotational levels. As for the ground electronic state of CeO^- , we predict the extra electron mainly reside in the 6s orbital of Ce forming the single particle electron configuration of $\sigma^2\sigma^{*2}\text{f}^1$ in the LFT framework. The $4f^1$ electron core with $^2\text{F}_{2.5}$ is unchanged and the ground state of CeO^- is then characterized as $X_{1.2.5}$ ($J_a=2.5$, $\Omega=2.5$) since the 6s (or σ^*) orbital is doubly occupied. The electron affinity of CeO is estimated to be 1.00(1) eV. The β value of the main band is 0.97(5), which is close to that of LaO^- , indicating that the 4f electron in CeO^- has little bearing on the detached electron. The band centered at 1.10 eV with $\beta \approx 0.19(5)$ is also assigned as exciting the Ce–O stretching mode of the neutral CeO molecule. Since the two lowest states of CeO have similar vibrational intervals ($\Delta G_{1/2}=824.3 \text{ cm}^{-1}$ for X_{12} and $\Delta G_{1/2}=824.02 \text{ cm}^{-1}$ for X_{23}) [57], the vibrational frequency of the ground state CeO is estimated to be $836(30) \text{ cm}^{-1}$ which is close to the experimental value of 808.3 cm^{-1} in solid noble gas matrix [58, 59]. Similar to that of LaO^- , the broad feature around 0.91 eV with $\beta \approx 1.85(15)$, is assigned as the hot band. The band gap between the first two bands gives an estimation of the stretching mode of CeO^- to be $750(60) \text{ cm}^{-1}$.

C. PrO^-

Figure 1(c) shows the photoelectron spectrum of PrO^- . There are two well resolved peaks labeled as X_1 and X_2 , located at 1.00 and 1.02 eV, with β value of 1.21(3) and 1.04(3), respectively. The band gap between the two peaks is about 25 meV (202 cm^{-1}), which is close to the first electron exciting energy (220 cm^{-1}). Thus, we assign the two peaks to the transitions to the ground state X_1 ($\Omega=3.5$) ($E=0 \text{ cm}^{-1}$) and first excited state X_2 ($\Omega=4.5$) ($E=220 \text{ cm}^{-1}$) of the neutral PrO , respectively [60, 61]. The characterizations of the two lowest electronic states are also from the LFT interpretation, similar to that of CeO mentioned above. Although spin-orbit coupling mixes other Hund's case (c) basis functions such as ($J_f=5$, $J_a=4.5$) in the LFT cal-

culation [23], the wave function ($J_c=4$, $J_a=3.5$) and ($J_c=4$, $J_a=4.5$) are the dominant components in the electronic wave functions X_1 ($\Omega=3.5$) and X_2 ($\Omega=4.5$), respectively. As the first approximation, we can also roughly characterize the two lowest lying states as X_1 ($J_a=3.5$, $\Omega=3.5$) and X_2 ($J_a=4.5$, $\Omega=4.5$) [10, 22, 61]. The separation of the ground state and the first excited state of PrO (220 cm^{-1}) comes from the difference in the orientation of the angular momenta of the $4f^2$ electron core and the spin of 6s electron. The ground state of PrO^- is characterized as X_1 ($J_a=4$, $\Omega=4$). The extra electron adds to 6s orbital of Pr and forms configuration $\text{Pr}^+(4f^26s^2)\text{O}^{2-}$ or $\sigma^2\sigma^{*2}\text{f}^2$ in the LFT framework. The electron affinity of PrO is determined to be 1.00(1) eV from the peak X_1 and is almost the same as that of CeO. The two not well resolved peaks located at 1.097(3) and 1.122(2) eV with whole $\beta \approx 0.25(3)$, are assigned as the exciting the Ce–O stretching mode of the neutral at X_1 ($\Omega=3.5$) and X_2 ($\Omega=4.5$) states, respectively. The vibrational frequencies of the two states are almost the same with a value of $815(30) \text{ cm}^{-1}$ which matches the matrix isolation experimental value (816.9 cm^{-1}) very well [58, 59]. The feature around 0.93 eV with $\beta \approx 1.85(15)$, is assigned as the hot band. It is hard to estimate the vibrational frequency of the PrO^- due to the flat and broad band and there are at least two transitions from the excited states of the anion to the ground state of the neutral in the hot band region.

D. NdO^-

Figure 1(d) shows the photoelectron spectrum of NdO^- . There are three main broad peaks observed in the spectrum. The peak X_1 corresponding to the transition to the ground state of NdO ($X(1)4$) [62], determines the electron affinity of NdO to be 1.01(1) eV with $\beta=0.45(1)$. The peak X_2 , located at 1.06(1) eV with $\beta=0.30(3)$, is assigned to the transition to the first excited state of NdO ((1)5) [62]. The band space between the two peaks is about 462 cm^{-1} (57.3 meV) which is close to the value of $473.691(1) \text{ cm}^{-1}$ got from the near-infrared emission spectra [62]. The NdO has a dominant $\text{Nd}^{2+}(4f^36s^1)\text{O}^{2-}$ ground state configuration under the purely ionic bonding model of LFT. The two wave functions under the Hund's case (c), ($J_c=4.5$, $J_a=4$) and ($J_c=4.5$, $J_a=5$) [23], are the dominant part of two lowest states wave functions of NdO, respectively. We can also roughly re-label the ground state and the first excited state of NdO as X_1 ($J_a=4$, $\Omega=4$) and X_2 ($J_a=5$, $\Omega=5$) to the first approximation, for a better comparison with the other LnO species mentioned above. The different angular momenta orientation of the $4f^3$ electron core and the 6s electron contributes to the band gap between the X_1 and X_2 peak of NdO. As for NdO^- , the extra electron is predicted to mainly reside in the 6s orbital of Nd. The ground electron configuration of NdO^- is $\sigma^2\sigma^{*2}\text{f}^3$ under the purely ionic bonding model of LFT and the ground state of NdO^- can be char-

TABLE III Natural atomic orbitals analysis of the anionic and neutral early lanthanide monoxides, including the natural charge on the metal atoms, calculated at the B3LYP and M06 levels.

	LaO ⁻		CeO ⁻		PrO ⁻		NdO ⁻	
	B3LYP	M06	B3LYP	M06	B3LYP	M06	B3LYP	M06
6s	1.86	1.86	1.86	1.86	1.86	1.86	1.86	1.86
5d	0.72	0.74	0.73	0.75	0.70	0.75	0.73	0.71
4f	0.17	0.19	1.20	1.22	2.25	2.24	3.20	3.29
Charge	0.21	0.20	0.17	0.15	0.14	0.13	0.16	0.11
	LaO		CeO		PrO		NdO	
	B3LYP	M06	B3LYP	M06	B3LYP	M06	B3LYP	M06
6s	0.92	0.93	0.92	0.93	0.92	0.93	0.92	0.87
5d	0.76	0.77	0.79	0.79	0.76	0.77	0.79	0.76
4f	0.19	0.21	1.22	1.25	2.28	2.29	3.23	3.35
Charge	1.13	1.12	1.07	1.06	1.03	1.02	1.04	1.02

acterized as X₁4.5 ($J_a=4.5$, $\Omega=4.5$). As can be seen in Fig.1(d), there is no sign of vibrational level of the ground electronic state of NdO, which is different from those in Fig.1 (a), (b), and (c). The broad feature centered at 0.91 eV with $\beta\approx 1.10(3)$, is assigned to the hot band and the vibrational frequency of NdO⁻ is estimated to be 787(40) cm⁻¹.

E. Comparison of EAs of the four species

Although the EA increases monotonically with the lanthanide atomic number, the EA of NdO is only 0.02 eV larger than that of LaO. The lanthanide monoxides (Ln=La, Ce, Pr, Nd) have similar EA, indicating that the four species have almost the same bonding character and the 4f electrons have little effect on the EA of the four early lanthanide monoxides. Comparing with the band gaps or the first exciting energies of the three lanthanide monoxides (CeO, PrO, NdO), 4f–6s exchange splitting exhibits a smooth variation with atomic number. There are three 4f electrons in NdO which exhibit the largest 4f–6s exchange splitting among the three 4f-electron-contained lanthanide monoxides. There is no obvious difference in the values of β for peak X₁ in the spectra of LaO, CeO, and PrO, while the β value of peak X₁ in the spectrum of NdO is much smaller than those of the other three, reflecting different or stronger 4f electron influence on behavior of the photodetached electron.

The theoretical results of LnO (Ln=La, Ce, Pr, Nd) are shown in Table II. The traditional hybrid functionals such as B3LYP and BP86 underestimate the electron affinities by about 0.1 eV. However, the calculated EAs from the new hybrid meta exchange-correlation functionals, called M06 and M06-2X, are in good agreement with the experimental results except for NdO. It should be noted that the M06-2X functional performs best among the investigated density functional methods [48], although it is parameterized only for nonmetals.

Only the EAs and vibrational frequencies given by the B3LYP and M06-2X methods show the same trend as the experimental values.

F. Natural population analysis

Natural population analysis was performed on the anionic and neutral lanthanide monoxides, and the results are listed in Table III. The natural atomic orbital occupancies calculated at the four density functional levels are similar to each other. Only the results at the B3LYP and M06 levels are displayed here as B3LYP is the most popular functional and M06 is parameterized including both transition metals and nonmetals [48]. Our results at the B3LYP level are similar to those previously reported using the same functional. It is interesting to see that the four diatomic anions have almost the same natural atomic orbital occupancies on 6s and 5d, and natural charge on the metal atoms. The difference in 4f occupancy comes from the original occupancy of 4f orbital in the lanthanide atoms. The inner Ln 4f-shell has a fractional electron population which is larger than formal population in the neutral atoms. The situations are the same for the four neutral species. Comparing the natural atomic orbital occupancies of 4f in the anionic with that of the corresponding neutral one, the 4f electrons tend to be localized and suffer little from the charge difference of the molecules.

According to the natural charge on the metal atoms, the charge distribution of LnO⁻ and LnO can be expressed as Ln⁺ $^{\delta-1}$ O[−] $^{\delta}$ and Ln⁺ $^{\delta}$ O[−] $^{\delta}$, respectively, where $\delta=1.1\pm 0.1$, which deviates from the $\delta=2$ assumption used in LFT badly. However, the LFT has been successfully used to interpret the complex laser spectra and to predict the orders and energies of the low-lying states of the lanthanide-containing molecules including lanthanide monoxides [7, 10, 57, 63]. Comparing the natural charge populations of the anions with those of the corresponding neutrals, the photodetached electron

mainly comes from the nearly double occupied 6s orbital of the metal. LFT is still an effective method to analyze the electronic state of LnO^- with the ground state configuration $\sigma^2\sigma^{*2}\text{f}^n$ under the purely ionic bonding model as discussed above.

IV. CONCLUSION

We report a combined photoelectron imaging and density functional theoretical study on the four early lanthanide monoxides, including LaO^- , CeO^- , PrO^- , and NdO^- . The well resolved photoelectron spectrum allows the EAAs to be determined as 0.99(1) eV for LaO , 1.00(1) eV for CeO , 1.00(1) eV for PrO , and 1.01(1) for NdO , respectively. The stretching frequencies of the neutral and anionic diatomic molecules are also reported. The EA increases monotonically with the lanthanide atomic number due to the increasing 4f electrons and the relativistic effect of the lanthanide atoms. The ground electronic states and configurations of the neutral and charged lanthanide monoxides are obtained by the LFT based on the purely ionic model that $\text{Ln}^{2+}\text{O}^{2-}$ arises from $\text{Ln}^{2+}4\text{f}^n6\text{s}$ and $\text{Ln}^{1+}\text{O}^{2-}$ arises from $\text{Ln}^{1+}4\text{f}^n6\text{s}$ ($n=0-3$ for La-Nd). Density functional calculations show that the new M06-2X functional implemented in Gaussian 09 has the best performance for the early lanthanides monoxides although it is a high-nonlocality functional and parameterized only for non-metals. Natural atomic orbital analyses give charge distribution of LnO^- and LnO expressed as $\text{Ln}^{+\delta-1}\text{O}^{-\delta}$ and $\text{Ln}^{+\delta}\text{O}^{-\delta}$, respectively, where $\delta=1.1\pm0.1$ and the 4f electrons tend to be localized and suffer little from the charge state of the molecules. The photodetached electrons mainly come from the 6s orbital of the metals. Although the LFT has the assumption of $\delta=2$, it is still an useful method to analyze the ground states of the neutral and anionic lanthanide monoxides.

V. ACKNOWLEDGMENTS

This work was supported by the National Natural Science Foundation of China (No.20933003) and the National Basic Research Program of China (No.2010CB732306).

- [1] M. R. Gagne, C. L. Stern, and T. J. Marks, *J. Am. Chem. Soc.* **114**, 275 (1992).
- [2] M. A. Giardello, Y. Yamamoto, L. Brard, and T. J. Marks, *J Am Chem Soc.* **117**, 3276 (1995).
- [3] C. D. Eads, P. Mulqueen, W. D. Horrocks, and J. J. Villafranca, *J. Biol. Chem.* **259**, 9379 (1984).
- [4] W. J. Liu, W. H. Xu, and Y. Zhang, *Sci. China Ser B* **52**, 1945 (2009).
- [5] P. Carette, *J. Mol. Spectrosc.* **140**, 269 (1990).

- [6] L. A. Kaledin, J. C. Bloch, M. C. McCarthy, L. V. Gurvich, and R. W. Field, *Mol. Phys.* **83**, 881 (1994).
- [7] C. Linton, M. Dulick, R. W. Field, P. Carette, P. C. Leyland, and R. F. Barrow, *J. Mol. Spectrosc.* **102**, 441 (1983).
- [8] C. Linton, M. Dulick, R. W. Field, P. Carette, and R. F. Barrow, *J. Chem. Phys.* **74**, 189 (1981).
- [9] Shenyavs. Ea, I. V. Egorova, and V. N. Lupanov, *J. Mol. Spectrosc.* **47**, 355 (1973).
- [10] M. Dulick and R. W. Field, *J. Mol. Spectrosc.* **113**, 105 (1985).
- [11] L. A. Kaledin, E. A. Shenyavskaya, and I. Kovacs, *Acta Phys. Hung.* **54**, 189 (1983).
- [12] C. Linton, B. J. Guo, R. S. Rana, and J. A. Gray, *J. Mol. Spectrosc.* **126**, 370 (1987).
- [13] B. R. Yadav, S. B. Rai, and D. K. Rai, *J. Mol. Spectrosc.* **89**, 1 (1981).
- [14] A. N. Kulikov, L. A. Kaledin, A. I. Kobyliansky, and L. V. Gurvich, *Can. J. Phys.* **62**, 1855 (1984).
- [15] C. Linton, D. M. Gaudet, and H. Schall, *J. Mol. Spectrosc.* **115**, 58 (1986).
- [16] Y. C. Liu, C. Linton, H. Schall, and R. W. Field, *J. Mol. Spectrosc.* **104**, 72 (1984).
- [17] L. A. Kaledin and E. A. Shenyavskaya, *J. Mol. Spectrosc.* **133**, 469 (1989).
- [18] C. Linton, S. McDonald, S. Rice, M. Dulick, Y. C. Liu, and R. W. Field, *J. Mol. Spectrosc.* **101**, 332 (1983).
- [19] S. A. McDonald, S. F. Rice, R. W. Field, and C. Linton, *J. Chem. Phys.* **93**, 7676 (1990).
- [20] A. Bernard and C. Effantin, *Can. J. Phys.* **64**, 246 (1986).
- [21] C. Linton, *J. Phys. IV* **1**, 525 (1991).
- [22] R. W. Field, *Ber. Bunsen. Phys. Chem.* **86**, 771 (1982).
- [23] P. Carette and A. Hocquet, *J. Mol. Spectrosc.* **131**, 301 (1988).
- [24] M. Dulick, E. Murad, and R. F. Barrow, *J. Chem. Phys.* **85**, 385 (1986).
- [25] M. Kotzian, N. Rosch, and M. C. Zerner, *Theor. Chim. Acta* **81**, 201 (1992).
- [26] S. G. Wang and W. H. E. Schwarz, *J. Phys. Chem.* **99**, 11687 (1995).
- [27] S. G. Wang, D. K. Pan, and W. H. E. Schwarz, *J. Chem. Phys.* **102**, 9296 (1995).
- [28] W. J. Liu, G. Y. Hong, D. D. Dai, L. M. Li, and M. Dolg, *Theor. Chem. Acc.* **96**, 75 (1997).
- [29] M. Dolg, G. Y. Hong, and L. M. Li, *Chem. Phys. Lett.* **334**, 396 (2001).
- [30] Z. J. Wu, W. Guan, J. Meng, and Z. M. Su, *J. Clust. Sci.* **18**, 444 (2007).
- [31] J. Schamps, M. Bencheikh, J. C. Barthelat, and R. W. Field, *J. Chem. Phys.* **103**, 8004 (1995).
- [32] M. Aubert-Frecon, A. R. Allouche, and S. Y. Umanskiy, *J. Chem. Phys.* **124**, (2006).
- [33] M. Dolg, X. Y. Cao, and W. J. Liu, *Sci. China Ser B* **45**, 91 (2002).
- [34] X. Y. Cao and M. Dolg, *J. Chem. Phys.* **115**, 7348 (2001).
- [35] M. Dolg, H. Stoll, and H. Preuss, *J. Chem. Phys.* **90**, 1730 (1989).
- [36] M. Dolg, M. Hulsen, P. Link, and U. Ruschewitz, *Theor. Chem. Acc.* **129**, 367 (2011).
- [37] K. P. Huber and G. Herzberg, *Molecular Spectra and Molecular Structure, in: Constants of diatomic molecules*, Wiley, New York, 1979.

- molecules*, New York: Van Nostrand Reinhold, (1979).
- [38] R. Klingeler, N. Pontius, G. Luttgens, P. S. Bechthold, M. Neeb, and W. Eberhardt, Phys. Rev. A **65**, (2002).
- [39] R. Klingeler, G. Luttgens, N. Pontius, R. Rochow, P. S. Bechthold, M. Neeb, and W. Eberhardt, Eur. Phys. J. D **9**, 263 (1999).
- [40] Z. C. Tang, X. Wu, Z. B. Qin, H. Xie, X. H. Wu, and R. Cong, Chin. J. Chem. Phys. **23**, 373 (2010).
- [41] A. T. J. B. Eppink and D. H. Parker, Rev. Sci. Instrum. **68**, 3477 (1997).
- [42] V. Dribinski, A. Ossadtchi, V. A. Mandelshtam, and H. Reisler, Rev. Sci. Instrum. **73**, 2634 (2002).
- [43] M. J. Frisch, G. W. Trucks, H. B. Schlegel, G. E. Scuseria, M. A. Robb, J. R. Cheeseman, G. Scalmani, V. Barone, B. Mennucci, G. A. Petersson, H. Nakatsuji, M. Caricato, X. Li, H. P. Hratchian, A. F. Izmaylov, J. Bloino, G. Zheng, J. L. Sonnenberg, M. Hada, M. Ehara, K. Toyota, R. Fukuda, J. Hasegawa, M. Ishida, T. Nakajima, Y. Honda, O. Kitao, H. Nakai, T. Vreven, J. A. Montgomery Jr., J. E. Peralta, F. Ogliaro, M. Bearpark, J. J. Heyd, E. Brothers, K. N. Kudin, V. N. Staroverov, R. Kobayashi, J. Normand, K. Raghavachari, A. Rendell, J. C. Burant, S. S. Iyengar, J. Tomasi, M. Cossi, N. Rega, N. J. Millam, M. Klene, J. E. Knox, J. B. Cross, V. Bakken, C. Adamo, J. Jaramillo, R. Gomperts, R. E. Stratmann, O. Yazyev, A. J. Austin, R. Cammi, C. Pomelli, J. W. Ochterski, R. L. Martin, K. Morokuma, V. G. Zakrzewski, G. A. Voth, P. Salvador, J. J. Dannenberg, S. Dapprich, A. D. Daniels, Ö. Farkas, J. B. Foresman, J. V. Ortiz, J. Cioslowski, D. J. Fox, *Gaussian 09, Revision A02*, Pittsburgh, PA: Gaussian, Inc., (2009).
- [44] A. D. Becke, J. Chem. Phys. **98**, 5648 (1993).
- [45] C. T. Lee, W. T. Yang, and R. G. Parr, Phys. Rev. B **37**, 785 (1988).
- [46] A. D. Becke, Phys. Rev. A **38**, 3098 (1988).
- [47] J. P. Perdew, Phys. Rev. B **33**, 8822 (1986).
- [48] D. G. Truhlar and Y. Zhao, Theor. Chem. Acc. **120**, 215 (2008).
- [49] M. Dolg, H. Stoll, A. Savin, and H. Preuss, Theor. Chim. Acta **75**, 173 (1989).
- [50] T. H. Dunning, J. Chem. Phys. **90**, 1007 (1989).
- [51] R. A. Kendall, T. H. Dunning, and R. J. Harrison, J. Chem. Phys. **96**, 6796 (1992).
- [52] A. E. Reed, L. A. Curtiss, and F. Weinhold, Chem. Rev. **88**, 899 (1988).
- [53] C. Adamo and P. Maldivi, Chem. Phys. Lett. **268**, 61 (1997).
- [54] A. J. R. Heck and D. W. Chandler, Annu. Rev. Phys. Chem. **46**, 335 (1995).
- [55] T. C. Steimle and W. Virgo, J. Chem. Phys. **116**, 6012 (2002).
- [56] C. Linton, J. H. Chen, and T. C. Steimle, J. Phys. Chem. A **113**, 13379 (2009).
- [57] L. A. Kaledin, J. E. McCord, and M. C. Heaven, J. Mol. Spectrosc. **158**, 40 (1993).
- [58] L. Andrews and S. P. Willson, J. Phys. Chem. A **103**, 3171 (1999).
- [59] M. F. Zhou, Y. Gong, and L. Andrews, Chem. Rev. **109**, 6765 (2009).
- [60] W. J. Childs, Y. Azuma, and G. L. Goodman, J. Mol. Spectrosc. **144**, 70 (1990).
- [61] T. C. Steimle, H. L. Wang, C. Linton, and T. M. Ma, J. Phys. Chem. A **113**, 13372 (2009).
- [62] A. Bernard, E. A. Shenyavskaya, and J. Verges, J. Mol. Spectrosc. **222**, 240 (2003).
- [63] B. J. Guo and C. Linton, J. Mol. Spectrosc. **147**, 120 (1991).